Advanced Control Strategies for Induction Motors: A Simulation-Based Analysis

[1]Bhupendra Nema, [2]Prof Sagar Tomar
[1]Department of Electrical and Electronics, Oriental Institute of Science and Technology
[2]Department of Electrical and Electronics, Oriental Institute of Science and Technology
bhupendranema@rediffmail.com

* Corresponding Author: Bhupendra Nema

Abstract: *Induction motors are fundamental components in numerous industrial and commercial applications, providing essential mechanical power through electromagnetic induction. This paper offers a comprehensive exploration of various control strategies and optimization techniques tailored for induction motors. Beginning with an overview of induction motor principles and types, including single-phase and three-phase variants, the paper delves into the objectives of the research, primarily focusing on V/f control implementation and parameter optimization using Ant Colony Optimization (ACO). Methodology-wise, the study utilizes MATLAB/Simulink environment for modeling and simulation, encompassing motor control systems and pulse width modulation (PWM) techniques. The investigation involves comparative analyses of control systems under different operational scenarios, including constant speed, acceleration, and deceleration, highlighting the efficacy of proposed strategies. Results depict the advantages of ACO-based optimization over conventional methods in achieving stable and efficient motor operation.*

Keywords: *Induction motors, V/f control, Ant Colony Optimization (ACO), Pulse Width Modulation (PWM), Motor modeling, Simulation, Control system analysis.*

I. INTRODUCTION

Induction motors are ubiquitous in modern industrial and commercial applications, serving as the workhorses of various electromechanical systems. Renowned for their robustness, simplicity, and efficiency, these motors have revolutionized numerous sectors ranging from manufacturing and transportation to household appliances. Operating on the principle of electromagnetic induction, induction motors convert electrical energy into mechanical energy with remarkable reliability and effectiveness. Electric motors known as induction motors utilize alternating current (AC) to function, being driven by a rotating magnetic field. They consist of essential components such as a rotor, a stator, and coils, which facilitate the conversion of electrical energy into mechanical energy through electromagnetic induction. These AC induction motors boast high efficiency and versatility, with a relatively uncomplicated design that enables them to adapt to various electrical demands across different applications. Widely recognized as asynchronous motors, they serve as primary drivers in industries spanning manufacturing, transportation, petrochemicals, and power systems due to their robust build, ease of control, affordability, reliability, high overload capacity, and efficiency. However, given their prolonged operational durations, these motors are exposed to significant electrical and mechanical strains, necessitating vigilance against potential faults. Such faults may arise from inherent issues within the machinery or from operating conditions. Detecting faults early is crucial to prevent motor failures that can result in downtime and productivity losses. Consequently, there has been a surge in research interest focused on fault diagnosis in induction motors [1,2]. Effective fault diagnosis and condition monitoring are pivotal not only in mitigating substantial damages but also in prolonging machine lifespan, enhancing accessibility, and minimizing breakdown maintenance. Fault detection prevents unforeseen disruptions and catastrophic damages to the entire drive system, while condition monitoring leads to reduced maintenance expenses and heightened reliability [3-4].

Figure 1 Induction Motor

An induction motor, featuring only amortisseur windings, is termed as such. This type of motor is often regarded as the most straightforward electrical machine in terms of its construction. Its operation is based on the fundamental principle of electromagnetic induction. In essence, when the rotating magnetic field generated by the stator interacts with the stationary rotor, it induces an electromagnetic field within the rotor itself. This induced field then facilitates the conversion of electrical energy into mechanical energy, enabling the motor to perform its intended function. Induction motors are exceptionally prevalent across a diverse range of settings, including industrial, commercial, and residential environments. They are typically utilized as three-phase AC motors, owing to their reliability and efficiency in converting alternating current into mechanical power. Key features that distinguish induction motors include their robustness, simplicity in design, and versatility in application. Despite their straightforward construction, these motors are capable of powering a wide array of machinery and equipment, making them indispensable in various sectors of industry and daily life.

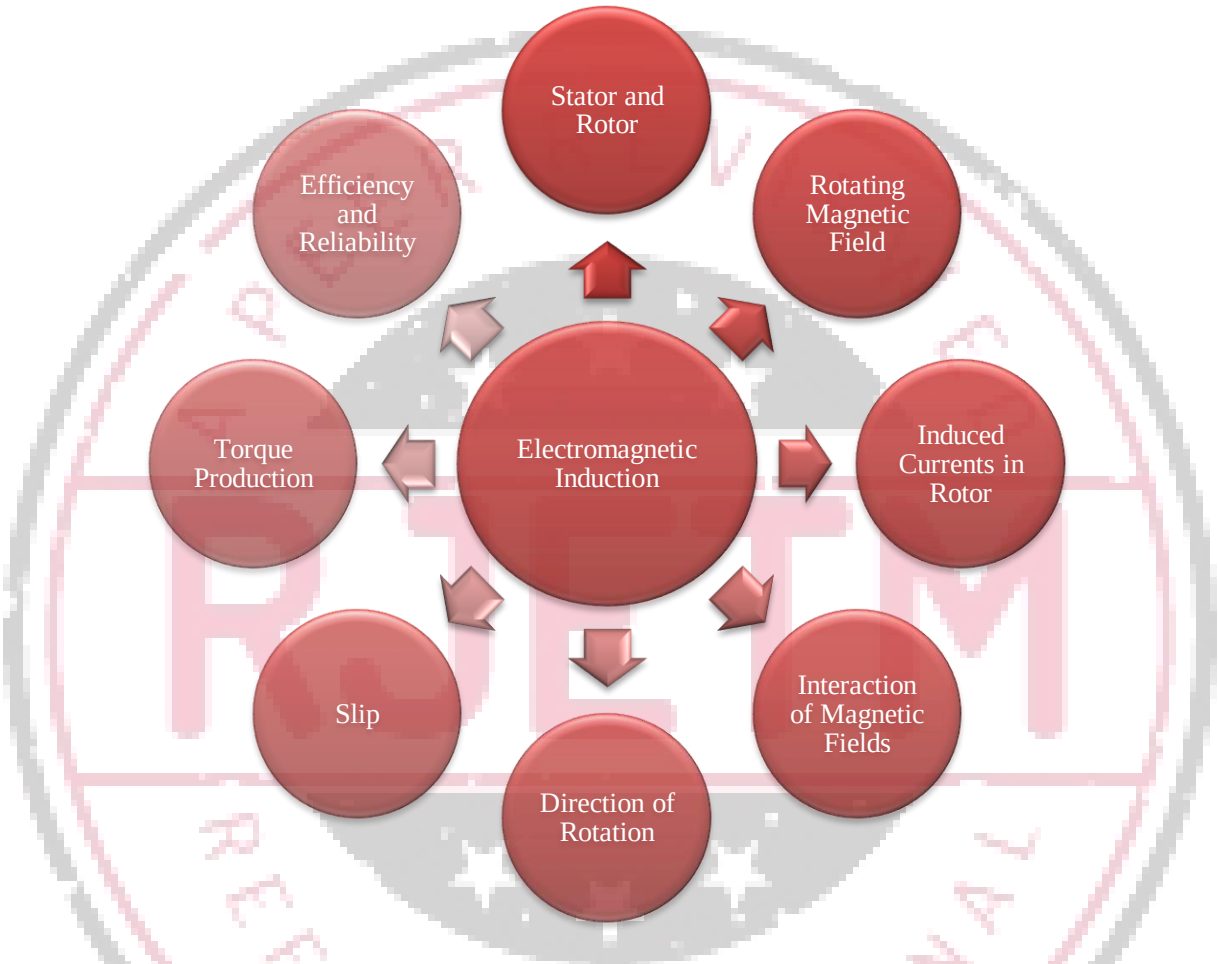

Figure 2 Operating principles of induction motors

Induction motors harness the principle of electromagnetic induction, where a dynamic magnetic field induces voltage in a conductor, leading to current flow. Consisting of a stationary stator and a rotating rotor, these motors generate a rotating magnetic field in the stator when supplied with alternating current, which in turn induces currents in the rotor. The interaction between these magnetic fields generates mechanical torque, propelling the rotor to rotate. The direction of rotation is dictated by the stator's rotating magnetic field. Slip, the variation from synchronous speed, enables torque generation necessary for driving loads. Renowned for their efficiency and reliability, induction motors are integral to diverse industrial and commercial applications, adept at converting electrical energy into mechanical power.

A. Types of Induction Motor

Single-phase induction motors and three-phase induction motors are the two primary types of induction motors. A single-phase induction motor runs by connecting to a single-phase AC power source, as their names suggest, whereas a three-phase induction motor needs a three-phase AC power source. Furthermore, each of these types of induction motors can be further subdivided into various subcategories. Single-phase motors are typically classified into four distinct types, while three-phase motors are generally divided into two main types.

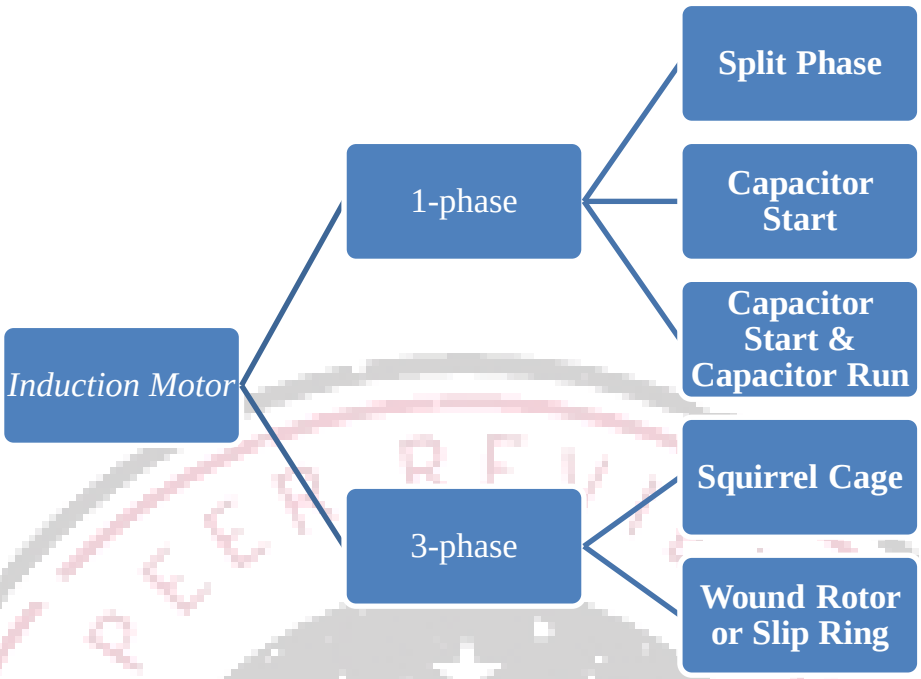

Figure 3 Types of Induction Motor

II. LITERATURE REVIEW

Marino et al. (2018) [5] developed a sophisticated control system for a fifth-order induction motor model, integrating input-output linearizing control with nonlinear adaptive feedback. This method accurately tracks load torque and rotor resistance by incorporating a nonlinear identification system. Once identified, the control algorithm optimizes rotor speed and flux amplitude regulation, enhancing power efficiency while maintaining speed control. Full state measurements are crucial for precise control across varying operating conditions.

Liang et al. (2020) [6] focused on fault diagnosis in induction motors using the finite element method (FEM). By modeling complex magnetic circuit topologies and material properties, FEM accurately determines machine parameters and detects faults, including localized saturation. Their review covers FEM-based fault diagnosis techniques, emphasizing its potential combined with signal processing and machine learning for comprehensive fault detection.

Yakhni et al. (2023) [7] investigated condition monitoring strategies for induction motors, particularly Transient Motor Current Signatures Analysis. They proposed two methods to address non-stationary signal frequencies and highlighted the importance of real-time fault detection to prevent sudden failures, especially in applications with varying speeds.

Aziz et al. (2023) [8] conducted a comprehensive examination of vector-controlled methods for induction motor drives, covering various control approaches and their impact on performance. They emphasized the significance of addressing uncertainties in motor parameters and highlighted the role of magnetic saturation and core loss. MATLAB simulations were utilized to demonstrate control strategies and their implications.

Karupusamy et al. (2023) [9] proposed a torque control drive analysis employing the Anticipating Power Impulse Technique (APIT) for speed regulation in induction motors. They mitigated issues like vibrations and singularities using sliding mode control and optimized parameters for improved performance and stability, validated through MATLAB simulations and experiments.

Biswas et al. (2023) [10] presented a novel pulse width modulation (PWM) approach for multilevel inverter-based induction motor driving, aiming to enhance power quality and reduce harmonic distortion. Their THI 2 SCPWM technique minimized power loss and torque ripple, improving dynamic response and overall performance, validated through simulations and experimental setups.

Tran et al. (2023) [11] introduced a failure recognition and correction approach for induction motors using deep learning and IoT, focusing on precise defect detection to prolong motor lifespan. Their method demonstrated resilience against false data attacks and outperformed existing algorithms in fault recognition, validated through experimental testing on real motors.

Attar et al. (2023) [12] conducted a comparative analysis of engine types for industrial robots, proposing a synchronous motor with permanent magnets based on mechanical design and application requirements. Their study highlighted the advantages of this design in terms of strength, torque, and performance, supported by simulations and comparisons with leading industry configurations.

Saxena et al. (2018) [13] investigated machine learning algorithms for health monitoring of three-phase induction motors, focusing on abnormal condition detection using CRNN approach. Their method outperformed other algorithms, offering improved recognition of abnormalities and compatibility with real-world applications.

IV. OBJECTIVES

The main objective of the thesis work is as follows:

- To develop a model or models to implement V/f control of an induction motor.
- Development of new optimization 'algorithm Ant Colony Optimization' (ACO) for tuning of the 'Proportional Integral '(PID) controller to achieve optimum speed control for Induction machine
- Study the speed torque waveforms for stability under various modes of operation, when the motor speed is constant, accelerating or decelerating.
- Compare the outcomes from the two algorithms namely V/F control and proposed parametric ant colony optimization control

IV METHODOLOGY

The model was crafted within the MALAB/SIMULINK environment, renowned for its prowess in scientific and engineering computation. This sophisticated platform operates at a high level, boasting a rich array of matrix and array capabilities alongside robust control flow statements, versatile functions, intricate data structures, and efficient input/output mechanisms. Its versatility extends to object-oriented programming, offering a comprehensive suite of features including:

- A high-level language tailored for scientific and engineering endeavors.
- A desktop environment finely tuned for iterative exploration, design, and effective problem-solving.
- Graphical tools facilitating data visualization and customizable plot creation.
- Specialized applications catering to tasks such as curve fitting, data classification, signal analysis, control system tuning, and beyond.
- Extensive add-on toolboxes catering to a diverse array of engineering and scientific domains.
- Utilities for constructing applications featuring tailor-made user interfaces.
- Flexible deployment options, allowing for the dissemination of MATLAB programs to end users without royalty constraints.

A. Motor Modeming and Simulation

Asynchronous machines currently stand as the most prevalent type of electrical machines, primarily employed as electrical induction motors and occasionally as generators. When the stator windings link up with a balanced three-phase network, a rotating magnetic field emerges. This rotational field arises from the flow of current through the coils and spins at a speed matching the frequency of the electrical power source connected to the stator. If this rotating magnetic field establishes a pair of poles (N, S) on the stator's surface, it signifies one cycle of alternating current (AC). In such instances, the count of pole pairs (P) corresponds to the number of these magnetic pairs.

$$f_1 = n_1/60 \qquad (4.1)$$

In order to delve into the mathematical model, it's customary to select one of the rectangular coordinate systems typically employed in this context [1, p 24]:

- The (α) and (β) coordinate system, anchored to the stator.
- The (d) and (q) coordinate system, affixed to the rotor and rotating synchronously with it.
- The (u) and (v) coordinate system, stationed on optional axes and revolving at an optional rate.

The power conversion process in electrical machines remains independent of the chosen coordinate system. Nonetheless, utilizing the (α) and (β) coordinate system is favored for studying power conversion equations due to the stator's voltage equations having a minimal number of terms. Additionally, in this coordinate system, the observer remains stationary in relation to the stator, and the network voltage frequency is accounted for.

To simulate the induction motor in MATLAB, the motor is represented by a set of equations and values according to the following steps:

B. Pulse Width Modulation and Converter Modeling

Principle of Pulse Width Modulation (PWM)

Fig 4.1 shows circuit model of a single-phase inverter with a centre-taped grounded DC bus, and Fig 4.2 illustrates principle of pulse width modulation.

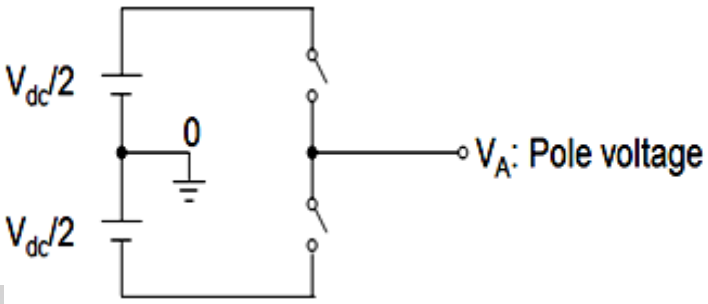

Figure 4 Circuit model of a single-phase inverter

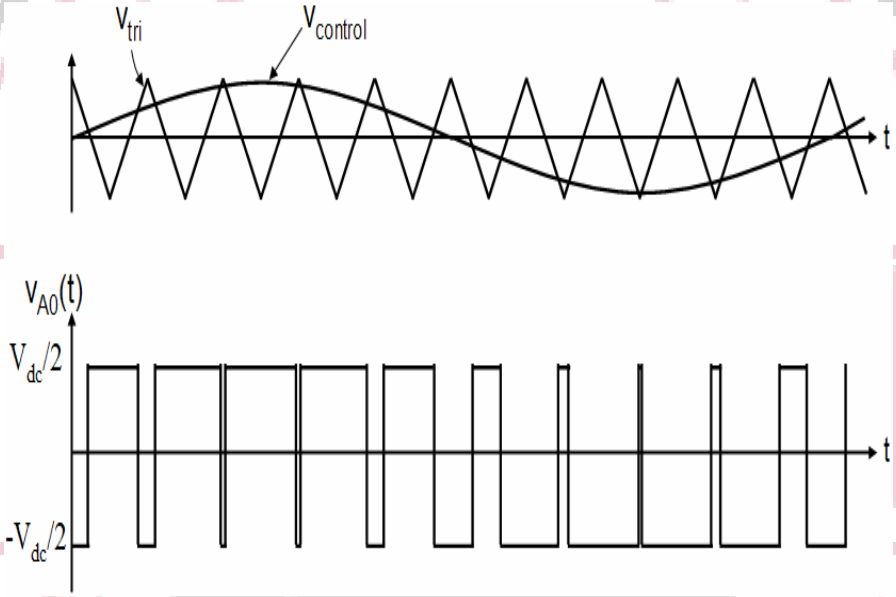

Figure 5 Generation of pulses in the control

As depicted in Fig 4. 2, the inverter output voltage is determined in the following

- When $V_{control} > V_{tri}$, $V_{A0} = V_{dc}/2$
- When $V_{control} < V_{tri}$, $V_{A0} = -V_{dc}/2$

Also, the inverter output voltage has the following features:

- PWM frequency is the same as the frequency of V_{tri}
- Amplitude is controlled by the peak value of $V_{control}$
- Fundamental frequency is controlled by the frequency of $V_{control}$

Principle of Sinusoidal PWM

Fig 5 shows circuit model of three-phase PWM inverter and Fig 4.4 shows waveforms of carrier wave signal (V_{tri}) and control signal ($V_{control}$), inverter output line to neutral voltages are V_{A0}, V_{B0}, V_{C0}, inverter output line to line voltages are V_{AB}, V_{BC}, V_{CA} respectively.

As described in Fig 4.4, the frequency of V_{tri} and $V_{control}$ is

- Frequency of $V_{tri} = f_s$
- Frequency of $V_{control} = f_1$

Where, f_s = PWM frequency and f_1 = Fundamental frequency

The inverter output voltages are determined as follows:

- When $V_{control} > V_{tri}$, $V_{A0} = V_{dc}/2$
- When $V_{control} < V_{tri}$, $V_{A0} = -V_{dc}/2$

Where, $V_{AB} = V_{A0} - V_{B0}$, $V_{BC} = V_{B0} - V_{C0}$, $V_{CA} = V_{C0} - V_{A0}$

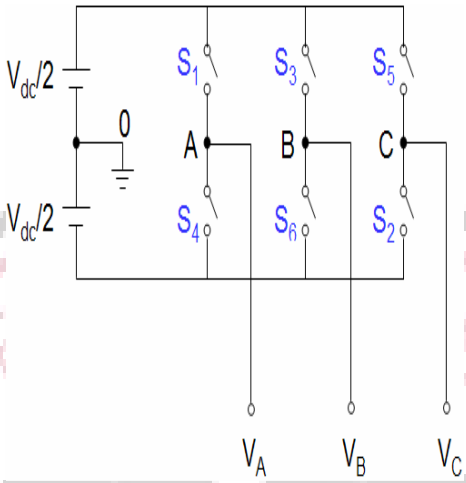

Figure 6 Three-phase PWM Inverterof general three-phase sine-PWM inverter

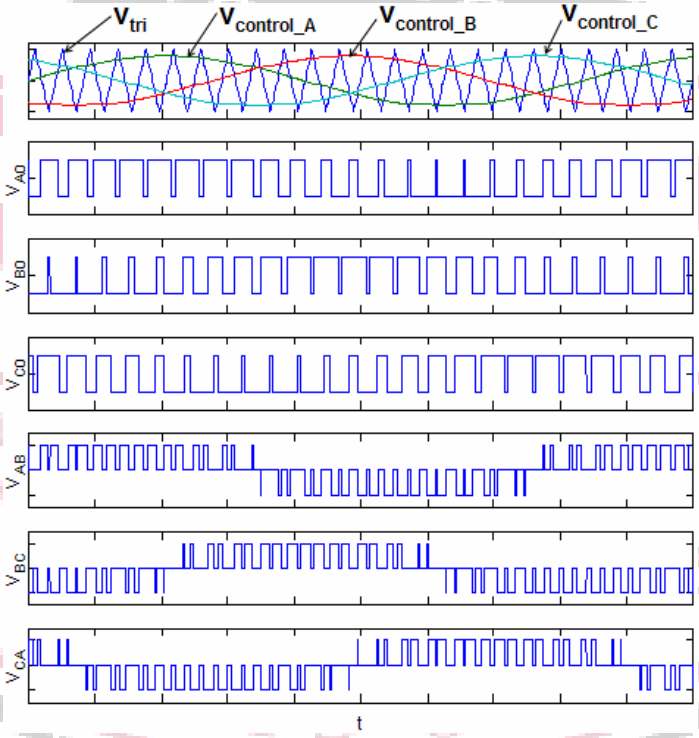

Figure 7 Reference signal generation for PWM

The inverter system described in this paper is a threephase grid connected three leg IGBTs based configuration commonly used in distributed generation interfaces. A synchronous frame PI current regulator was chosen to control the inverter.

When the generated power is transmitted to the grid, or used by AC loads, it is necessary to use DC-AC converters (inverters). Inverters can be single phase or three phase output. There are four common grid integrated inverters for photovoltaic systems: the central plant inverter system, the string inverter system, the multi-string inverter system, and microgrid inverter (AC modules) system.

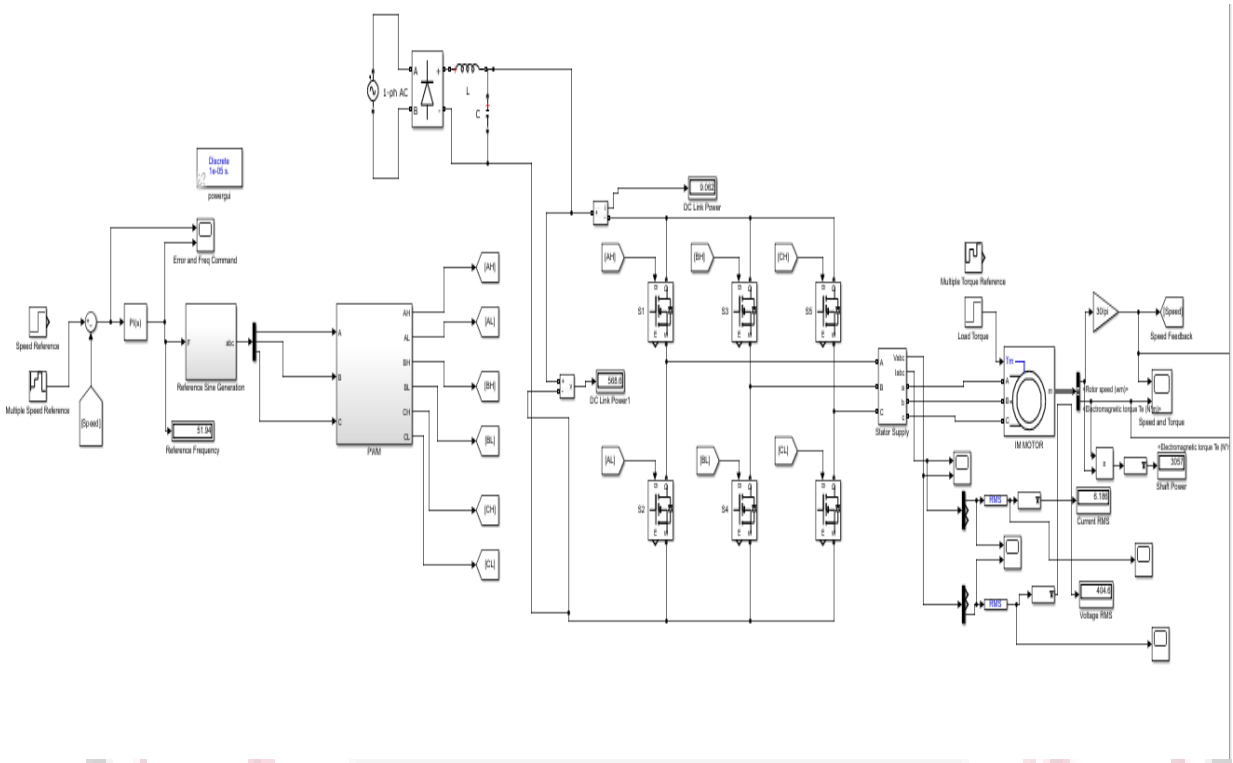

Figure 8 MATLAB/SIMULINK designing of three phase converter

The design of the inverter control aims to enhance system parameters. It is formulated in the dq0 reference frame for simplifying the analysis of individual components and their respective alterations. The system continually monitors variable parameters and adjusts them as necessary. This controller furnishes pulses to a three-leg 6-pulse inverter, utilizing motor speed parameters as inputs. Typically, the switching frequency remains constant. The operation is grounded on the triangular carrier wave principle of the desired switching frequency, compared with the error of the controlled signal. The error signal results from the summation of the reference signal generated within the controller and the negative feedback of the actual motor current from the motor. The voltage signal obtained triggers the gates of the voltage source inverter to produce the desired output. If the error command surpasses the carrier, the inverter leg remains switched to the positive polarity. Conversely, when the error command diminishes, the inverter leg switches to the negative polarity. This process generates the PWM signal, with the output voltage of the inverter being proportionate to the current error command.

C. V/F Motor Control System

In this control method, the motor receives variable frequency signals generated by PWM control from an inverter. Here, the V/f ratio is upheld as constant to maintain consistent torque across the entire operational spectrum. Since only the magnitudes of input variables—frequency and voltage—are regulated, this method is termed "scalar control." It offers a cost-effective and straightforward solution. Minimal knowledge of the motor is necessary for frequency control, making it widely adopted. However, a drawback of such control is that the developed torque depends on the load since it is not directly controlled. Additionally, the transient response is sluggish due to the predetermined switching pattern of the inverter. Continuous blockage to rotor rotation results in motor heating despite the implementation of overcurrent control loops. Incorporating a speed/position sensor can mitigate issues related to blocked rotors and load-dependent speeds but at the expense of increased system cost, size, and complexity. Various approaches exist for implementing scalar control. In closed-loop V/f Control, the rotor speed is sensed using a sensor and compared to a reference speed. The disparity serves as the error input to a Proportional controller, which adjusts the inverter frequency. This frequency becomes the input for the Voltage Source Inverter, regulating the terminal voltage to maintain a constant V/f ratio. The initial frequency for stable motor operation is computed, along with its corresponding voltage. Rotor speed is incrementally increased from 0 to synchronous speed, recording torque values at each step. The actual rotor speed is compared to the reference, correcting the frequency accordingly. Terminal voltage is adjusted to maintain the V/f ratio, and the process repeats. Torque and speed graphs are then plotted.

Consequently, the rotor speed is monitored and compared to the reference speed, generating an error signal processed by the Proportional Controller. This, in turn, adjusts the supply frequency, while the Voltage Source Inverter also adapts the voltage to uphold the constant V/f ratio. This stability in flux ensures a consistent maximum torque across the speed range, achieving speed control in the induction motor.

D. Ant Colony Based Parameters Optimization of the Motor Control

Ant Colony Optimization (ACO) is a discrete combinatorial optimization algorithm inspired by the collective behavior of ants in their search for food. Ant colonies are capable of finding the shortest routes from their nest to a food source through indirect communication, involving the deposition of a chemical substance known as pheromone on the paths they traverse. Over time, paths with shorter distances and higher desirability accumulate more pheromone, becoming the preferred routes for the colony. ACO functions as a metaheuristic algorithm where a colony of artificial ants collaborates to find optimal solutions for static and dynamic optimization problems across discrete and continuous domains. It distributes computational resources among a group of relatively simple agents, or artificial ants, which communicate indirectly through pheromone trails. This probabilistic multi-agent algorithm employs a probability distribution to transition between iterations. Although ant algorithms excel in solving discrete combinatorial optimization problems, their successful application in continuous search spaces has been widely documented.

The application of the ACO algorithm addresses various challenges encountered in problem-solving scenarios. It leverages insights from the biological inspiration and behavior of ant colonies, relating them to real-life problems. An instance of its application involves optimizing parameters in the design of a nonlinear proportional-integral (PI) controller. The ACO algorithm, inspired by real ant behavior, constructs an objective function based on position tracking error and employs an elitist strategy for optimization. Detailed simulation procedures are outlined, demonstrating the efficacy of the nonlinear PI controller optimized using the ACO algorithm. This controller exhibits precise control and rapid response, with the gains Kp and Ki dynamically generated by the ACO algorithm for a given system.

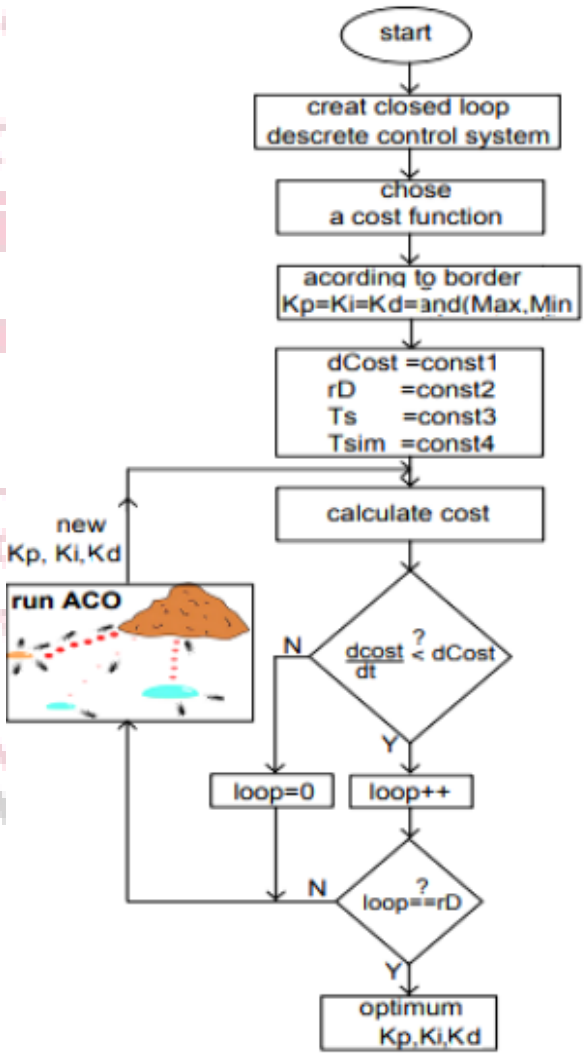

Figure 9 Ant colony implementation for speed control with parameter optimization

The Ant Colony Optimization (ACO) method is a metaheuristic technique designed to address a broad range of computational problems by integrating user-defined heuristics, with the aim of enhancing procedural efficiency. Employing the ACO method contributes to improving system stability and the quality of speed responses. In this particular investigation, the parameters Kp and Ki are optimized using the ACO heuristic optimization algorithm. The ACO algorithm evaluates the cost of the control process to facilitate the calculation of optimal controller parameters. This ACO-based

speed control strategy aims to continuously monitor and update system variations, ensuring the generation of improved pulses and enhanced output parameters at each stage.

V. RESULT AND DISCUSSION

The primary goal of the project is to create one or more models for implementing V/f control of an induction motor. To achieve this, it's essential to have a thorough understanding of the PWM inverter responsible for driving the induction motor. Therefore, the project also entails studying and simulating PWM signal generation techniques and various inverter topologies. The discussion will be based on a MATLAB simulation of different speeds of the induction motor. The induction motor model is created according to a group of standard equations (current, voltage, power, efficiency, speed) and values developed.

The first system being driven by conventional PI regulatory control and the other one is being modified to adjust the disturbances in the waveforms by using ACO algorithms.

Case 1: Analysis of the control system at constant speed

Case 2: Analysis of the control system with variation in speed (acceleration) at 3 sec

Case 3: Analysis of the control system with variation in speed (deceleration) at 3 sec

The speed and torque waveforms are being discussed in following four cases with three mode of operation, acceleration, constant drive and deceleration.

A. Case 1: Analysis of the control system at constant speed

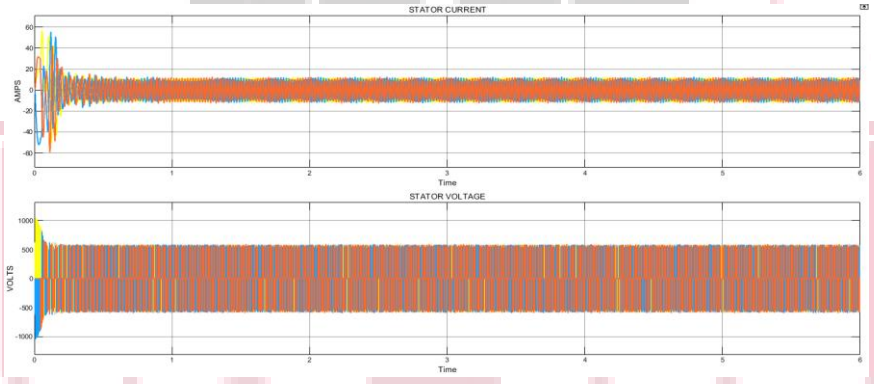

Figure 10 Three phase current and voltage waveforms in system 1 with basic V/F control (constant drive)

The representation of three phase voltage and current outputs when the motor speed is constant is represented in figure 10 in system 1 having speed controller driven by V/F control

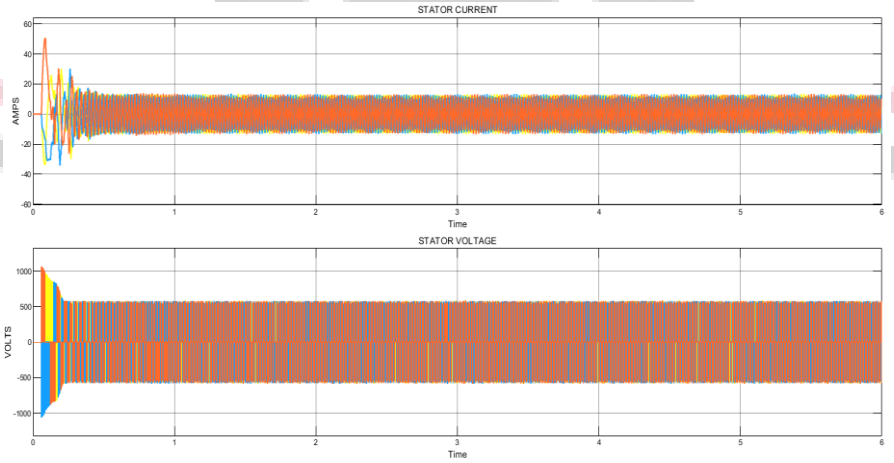

Figure 11 Three phase current and voltage waveforms in system 2 with parametric ant colony optimization control (constant drive)

The representation of three phase voltage and current outputs when the motor speed is constant is represented in figure 5.2 for system 2 having speed controller driven by parametric ant colony optimization control.

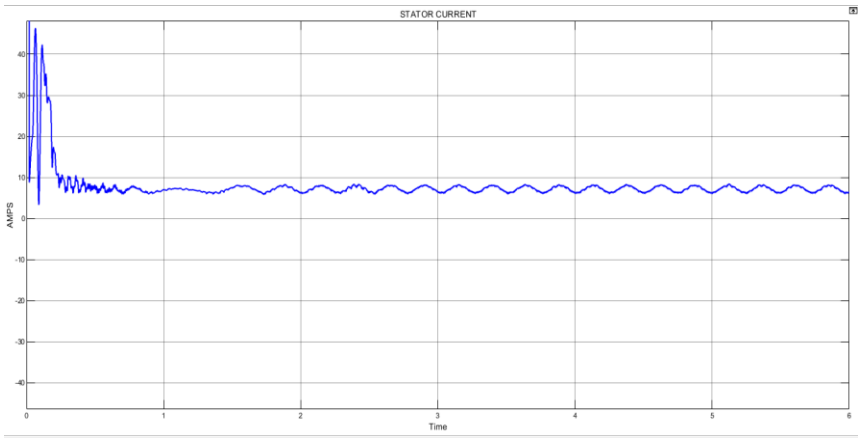

Figure 11 RMS current waveform representation in system 1 with basic V/F control (constant drive)

To analyse the variations in the current waveform the RMS value is calculated which is represented in figure 11. The graphs shows variations in the waveform in the system having V/F speed control of motor during constant drive.

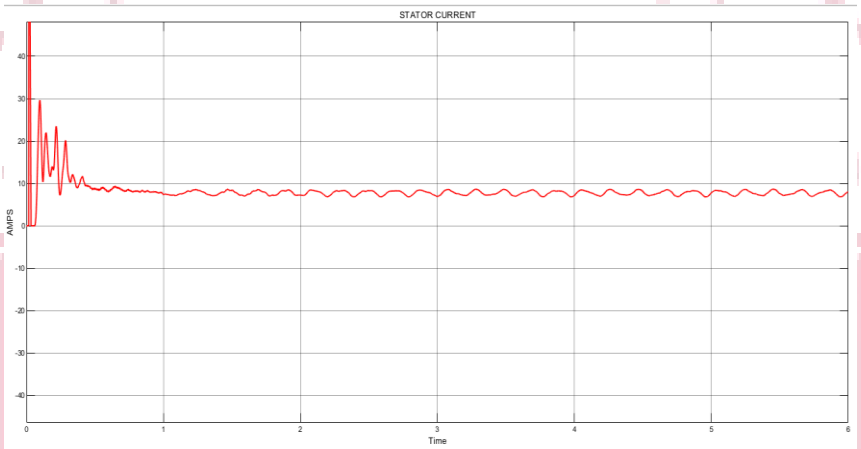

Figure 12 RMS current waveform representation in system 2 with parametric ant colony optimization control (constant drive)

To analyse the variations in the current waveform the RMS value is calculated which is represented in figure 12. The graphs shows less variations in the waveform in the system having proposed parametric ant colony optimization control during constant as compared to waveform in V/F controller

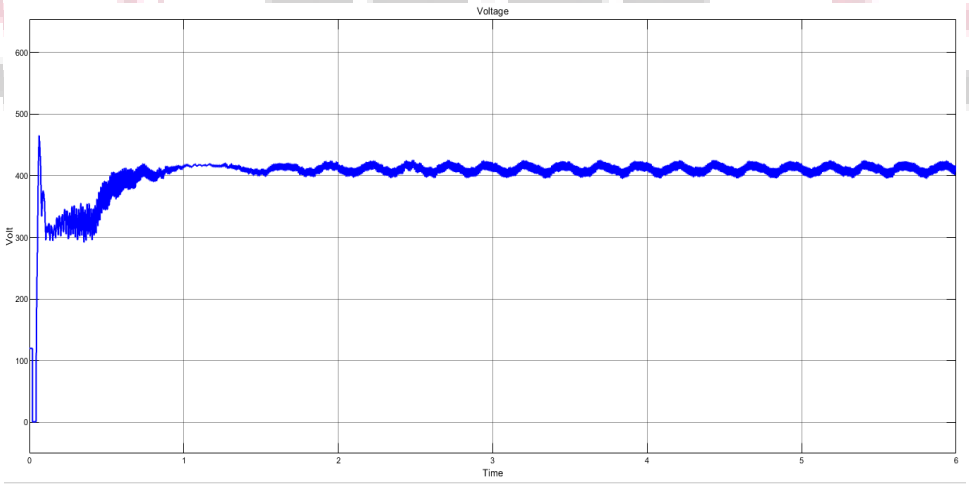

Figure 13 RMS voltage waveform representation in system 1 with basic V/F control (constant drive)

To analyse the variations in the voltage waveform the RMS value is calculated which is represented in figure 13. The graphs shows variations in the waveform in the system having V/F speed control of motor during constant drive mode.

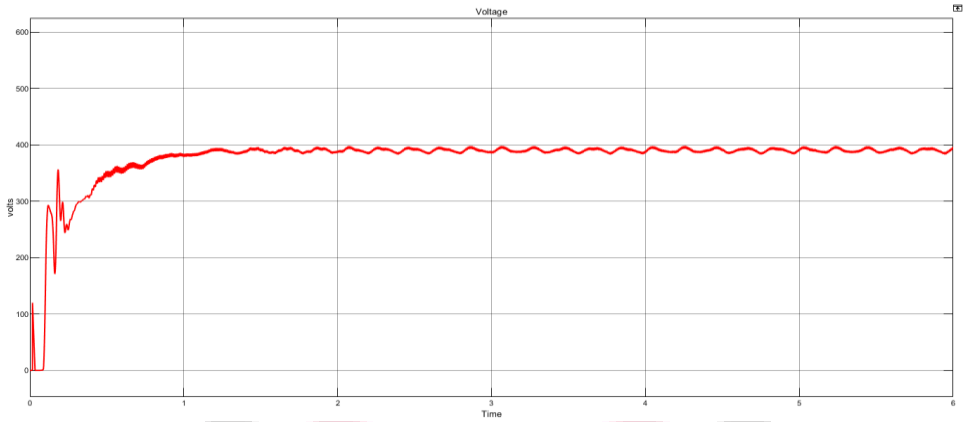

Figure 14 RMS voltage waveform representation in system 2 with parametric ant colony optimization control (constant drive)

To analyse the variations in the voltage waveform the RMS value is calculated which is represented in figure 14. The graphs shows less variations in the waveform in the system having proposed parametric ant colony optimization control during constant mode as compared to waveform in V/F controller

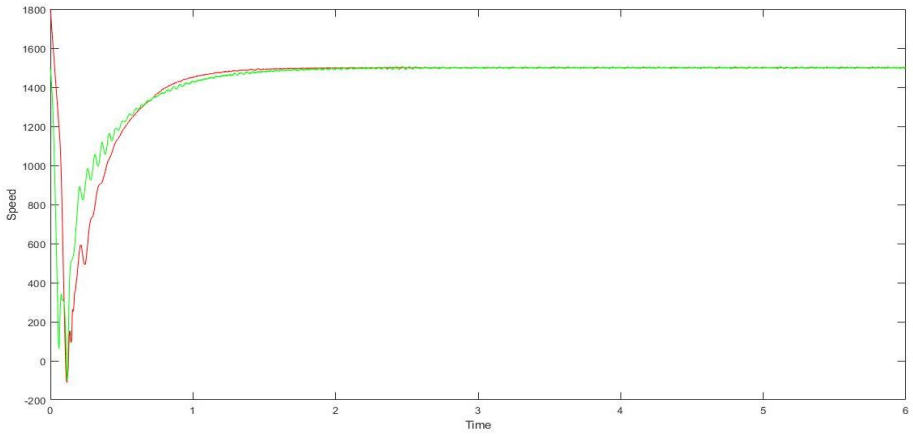

Figure 15 Comparative analysis of speed in the two systems in case 1 (constant drive)

The comparative analysis of the speed in the two systems with different control has been depicted in the figure 15. The green graphs represents the outcome from the system 1 with V/F control and the red graphs is the speed of the motor during constant drive in system 2 with proposed speed controller parametric ant colony optimization control.

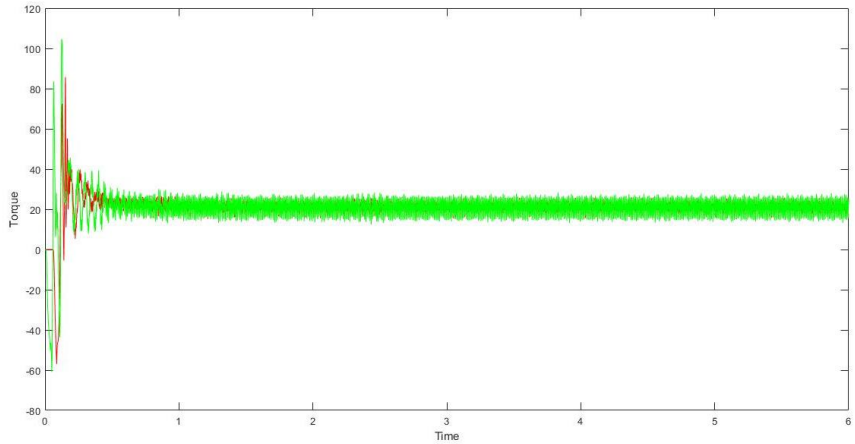

Figure 16 Comparative analysis of torque in the two systems in case 1 (constant drive)

The comparative analysis of the torque in the two systems with different control has been depicted in the figure 16. The green graph represents the outcome from the system 1 with V/F control and the red graphs is the torque produced in the motor during constant drive in system 2 with proposed speed controller parametric ant colony optimization control.

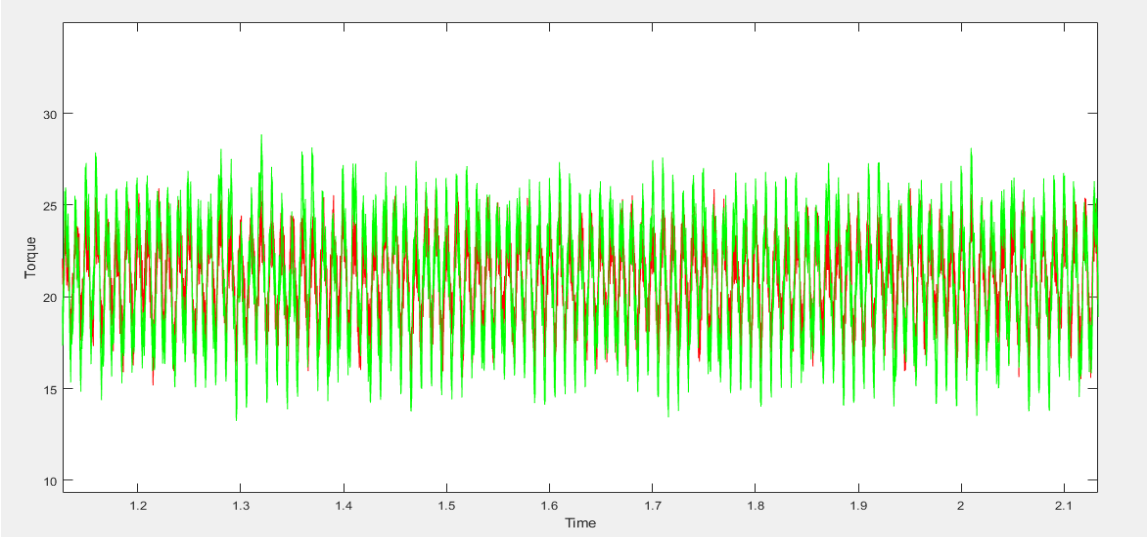

Figure 17 Close view of the torques in two systems in case 1 (constant drive)

Figure 17 is the comparative graph of torques in the two systems with closer view of the variations produced in them during constant drive mode. The green graph as shown is having more variable waveform when compared with the red one.

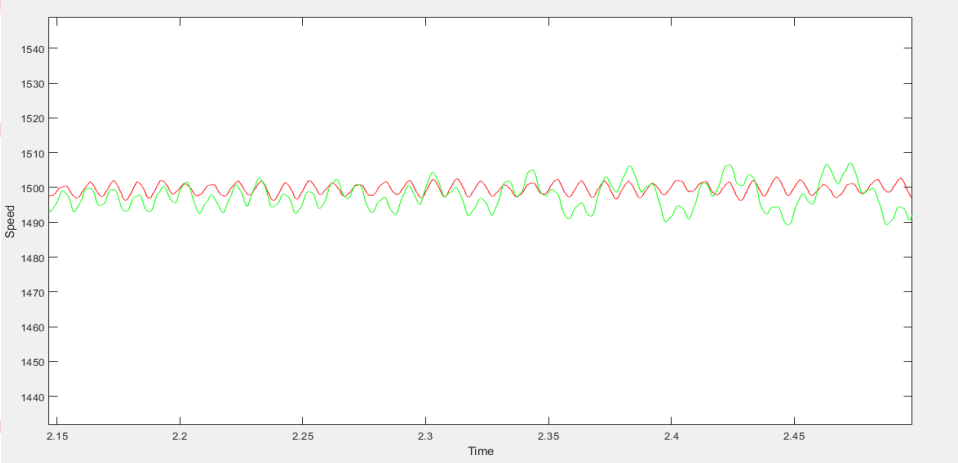

Figure 18 Close view of the speeds in two systems in case 1 (constant drive)

Figure 18 is the comparative graph of speeds in the two systems with closer view of the variations produced in them during constant drive mode. The green graph as shown is having more variable waveform when compared with the red one.

B. Case 2: Analysis of the control system with variation in speed (acceleration) at 3 sec

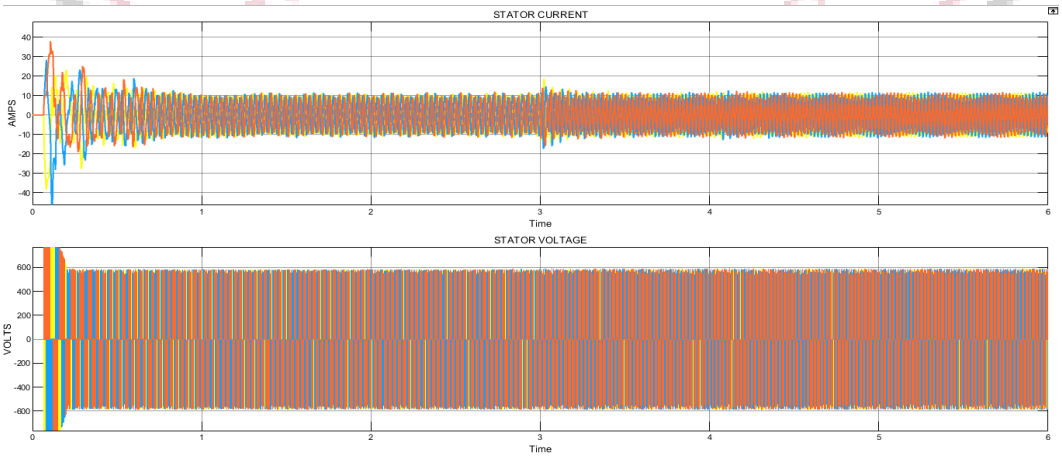

Figure 19 Three phase current and voltage waveforms in system 1 with basic V/F control (acceleration mode)

The representation of three phase voltage and current outputs when the motor speed is increased at 3 sec is represented in figure 19 in system 1 having speed controller driven by V/F control

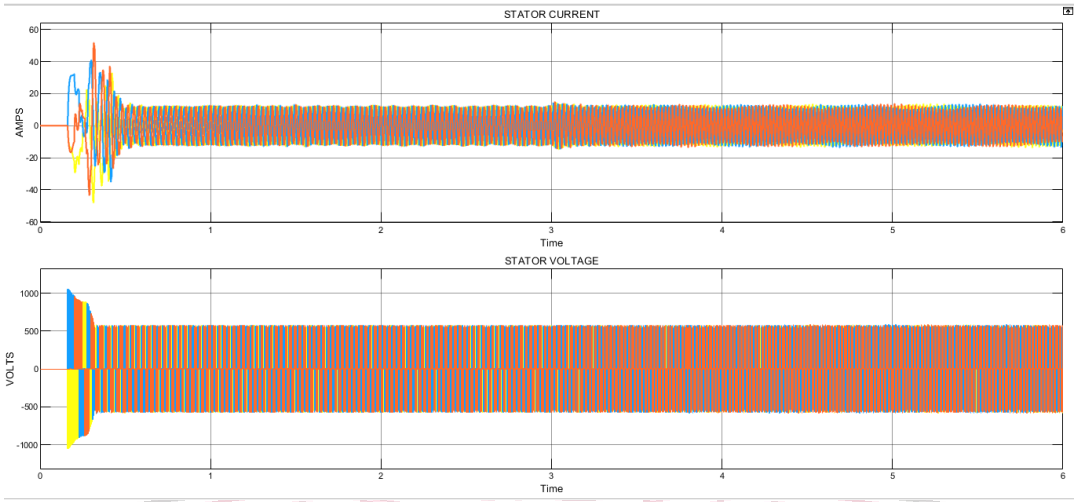

Figure 20 Three phase current and voltage waveforms in system 2 with parametric ant colony optimization control (acceleration mode)

The representation of three phase voltage and current outputs when the motor speed is increased at 3 sec is represented in figure 20 for system 2 having speed controller driven by parametric ant colony optimization control.

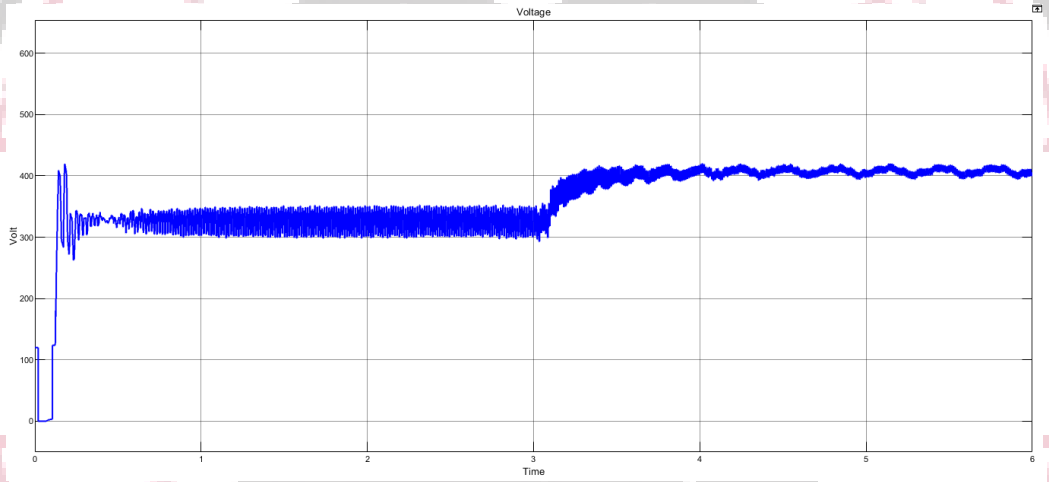

Figure 21 RMS voltage waveform representation in system 1 with basic V/F control (acceleration mode)

To analyse the variations in the voltage waveform the RMS value is calculated which is represented in figure 21. The graphs shows variations in the waveform in the system having V/F speed control of motor during acceleration at the 3 sec.

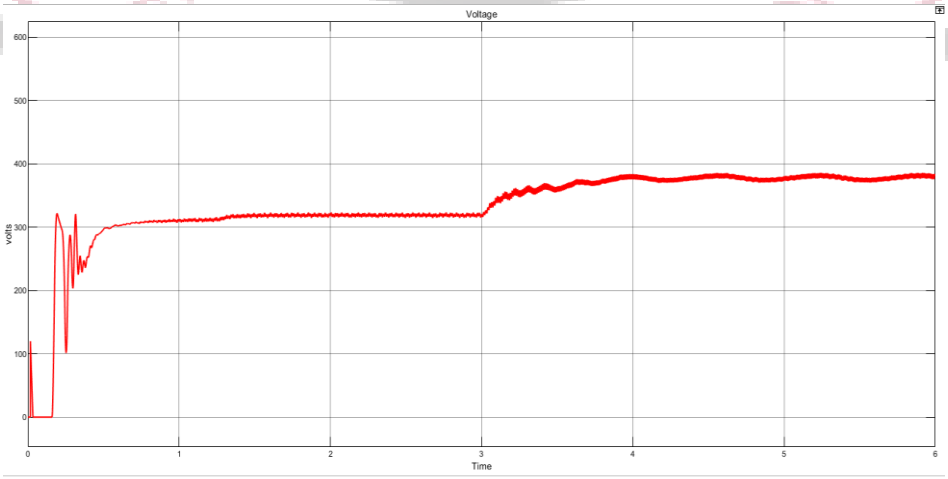

Figure 22 RMS voltage waveform representation in system 2 with parametric ant colony optimization control (acceleration mode)

To analyse the variations in the voltage waveform the RMS value is calculated which is represented in figure 22. The graphs shows less variations in the waveform in the system having proposed parametric ant colony optimization control during acceleration at 3 sec and then after wards its stabilizes more as compared to waveform in V/F controller

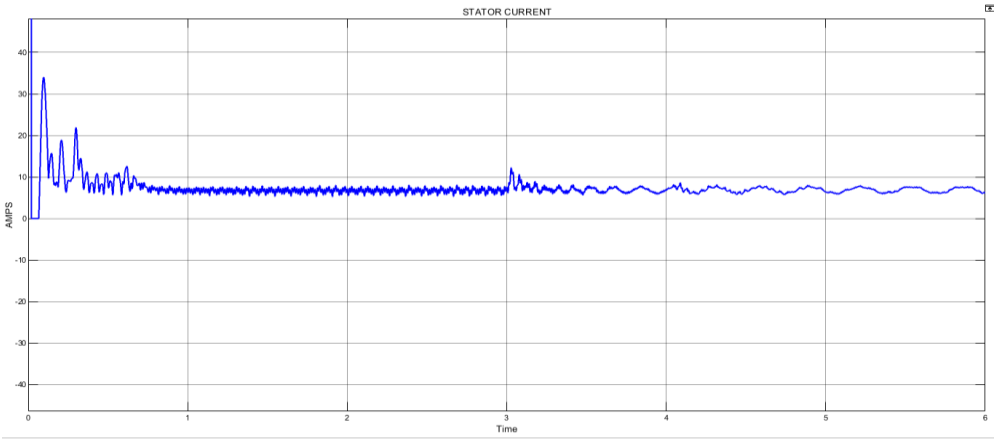

Figure 23 RMS current waveform representation in system 1 with basic V/F control (acceleration mode)

To analyse the variations in the current waveform the RMS value is calculated which is represented in figure 23. The graphs shows variations in the waveform in the system having V/F speed control of motor during acceleration at the 3 sec.

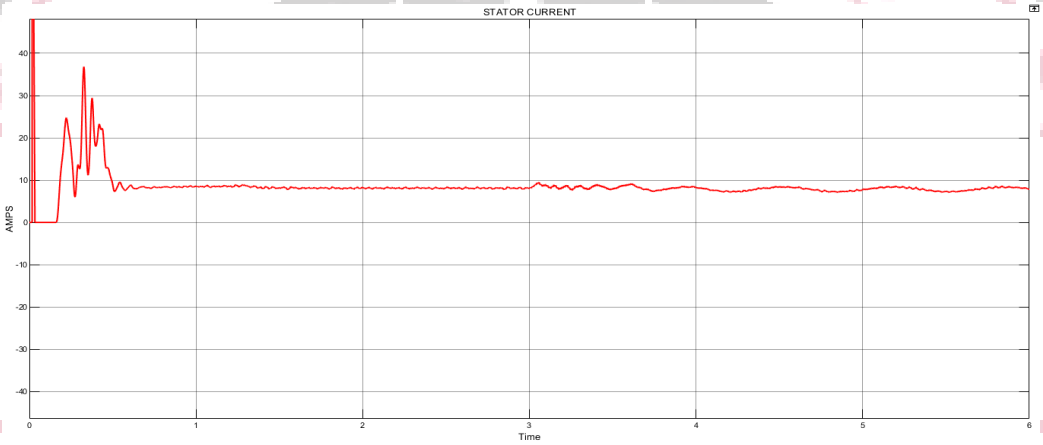

Figure 24 RMS current waveform representation in system 2 with parametric ant colony optimization control (acceleration mode)

To analyse the variations in the current waveform the RMS value is calculated which is represented in figure 24. The graphs shows less variations in the waveform in the system having proposed parametric ant colony optimization control during acceleration at 3 sec and then afterwards its stabilizes more as compared to waveform in V/F controller

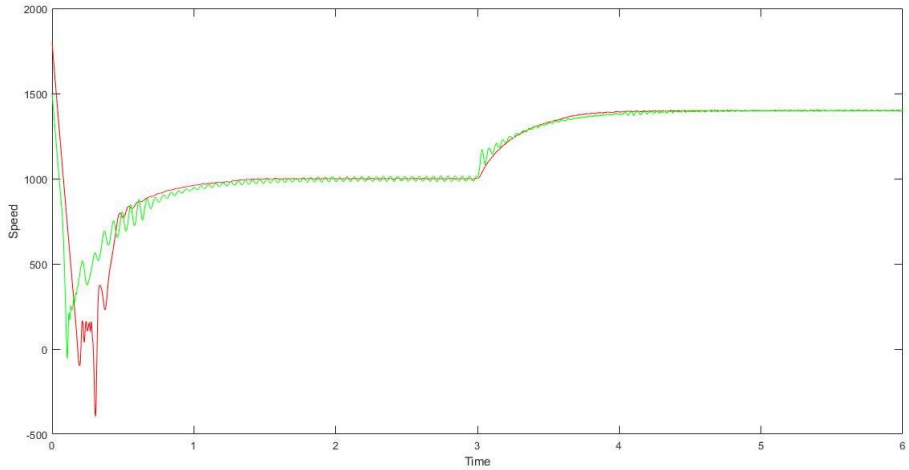

Figure 25 Comparative analysis of speeds in the two systems in case 2 (acceleration mode)

The comparative analysis of the speeds in the two systems with different control has been depicted in the figure 25. The green graph represents the outcome from the system 1 with V/F control and the red graph is the speed of the motor in system 2 with proposed speed controller parametric ant colony optimization control during acceleration produced at 3 sec.

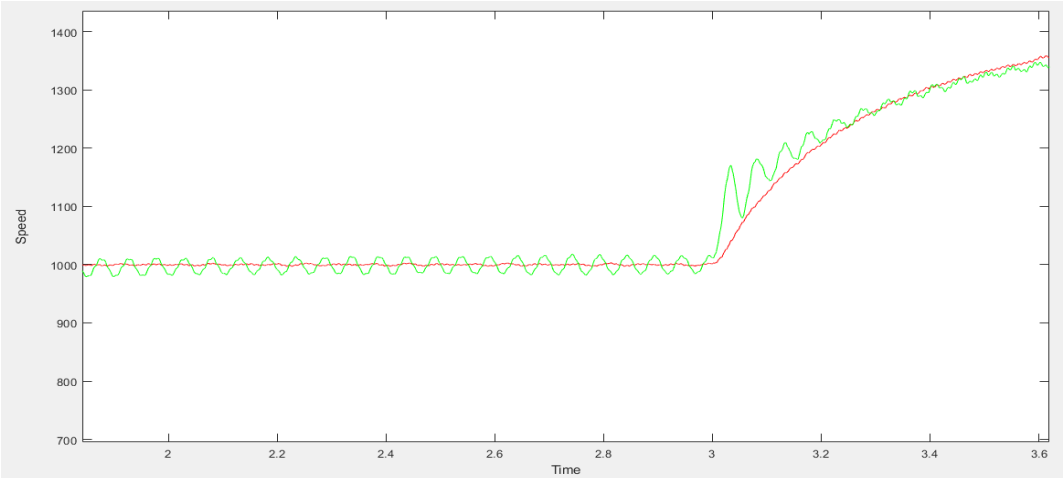

Figure 26 Close view of the speeds in two systems in case 2 (acceleration mode)

Figure 26 is the comparative graph of speeds in the two systems with closer view of the variations produced in them during acceleration mode. The green graph as shown is having more variable waveform when the speed is increased at 3 sec producing a spike and the red graph is increasingly more smoothly.

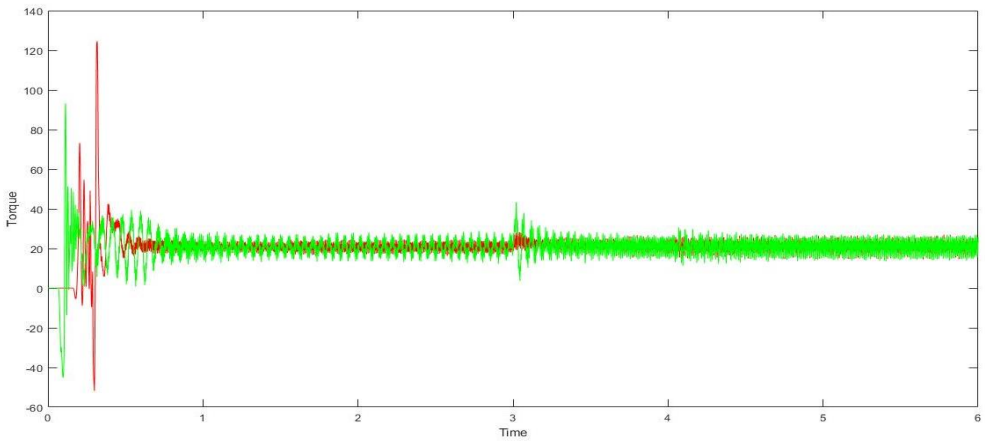

Figure 27 Comparative analysis of torque in the two systems in case 2 (acceleration mode)

The comparative analysis of the torques in the two systems with different control has been depicted in the figure 27. The green graph represents the outcome from the system 1 with V/F control and the red graph is the torque produced in motor in system 2 with proposed speed controller parametric ant colony optimization control during acceleration produced at 3 sec.

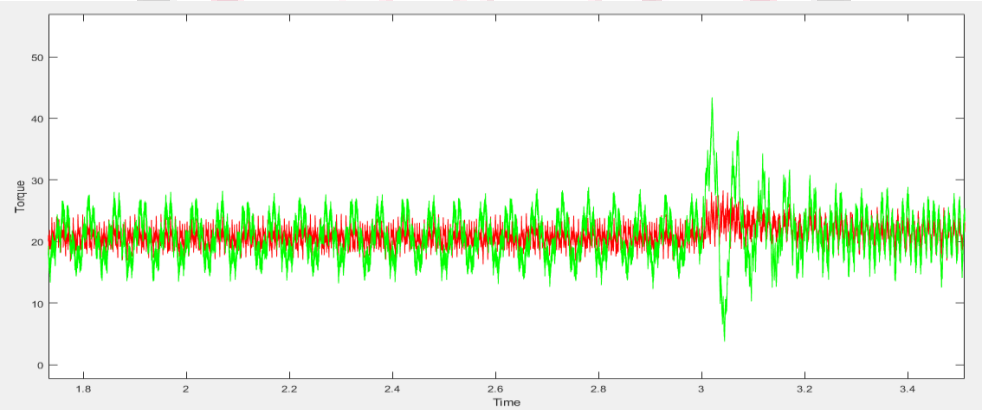

Figure 28 Close view of the torque in two systems in case 2 (acceleration mode)

The comparative graph of torques in the two systems with closer view of the variations produced in them during acceleration mode is presented in figure 28. The green graph as shown is having more variable waveform when the speed is increased at 3 sec producing a spike in torque also and the red graph of torque is more stable.

C. Case 3: Analysis of the Control System with Variation in Speed (Deceleration) at 3 sec

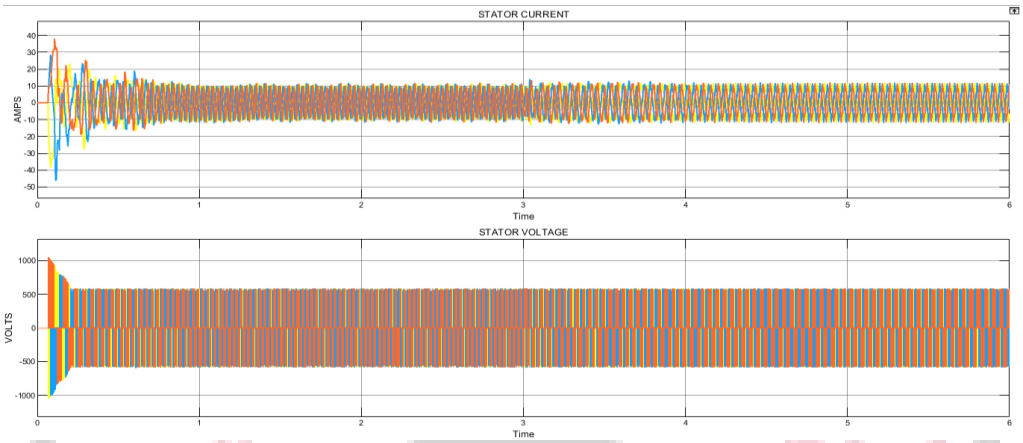

Figure 29 Three phase current and voltage waveforms in system 1 with basic V/F control (Deceleration mode)

The representation of three phase voltage and current outputs when the motor speed is decreased at 3 sec is represented in figure 29 in system 1 having speed controller driven by V/F control

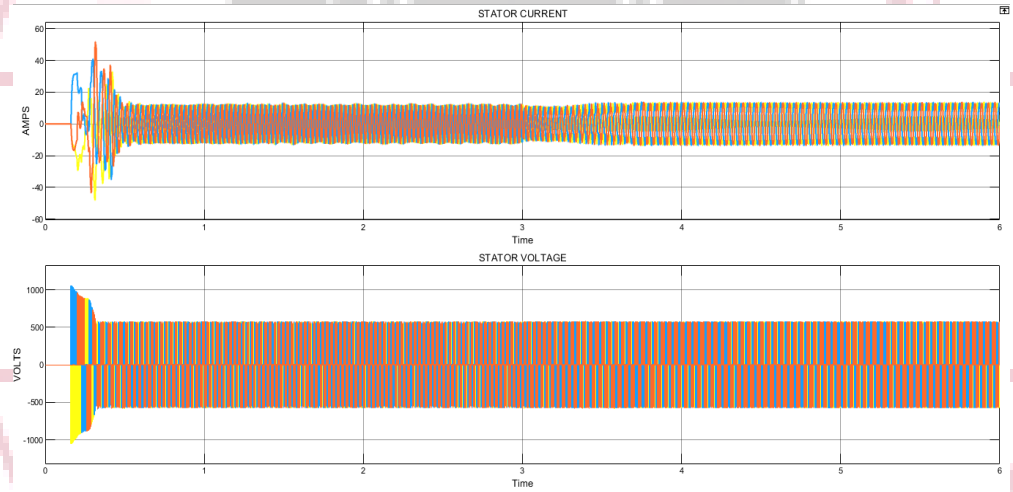

Figure 30 Three phase current and voltage waveforms in system 2 with parametric ant colony optimization control (Deceleration mode)

The representation of three phase voltage and current outputs when the motor speed is decreased at 3 sec is represented in figure 30 for system 2 having speed controller driven by parametric ant colony optimization control.

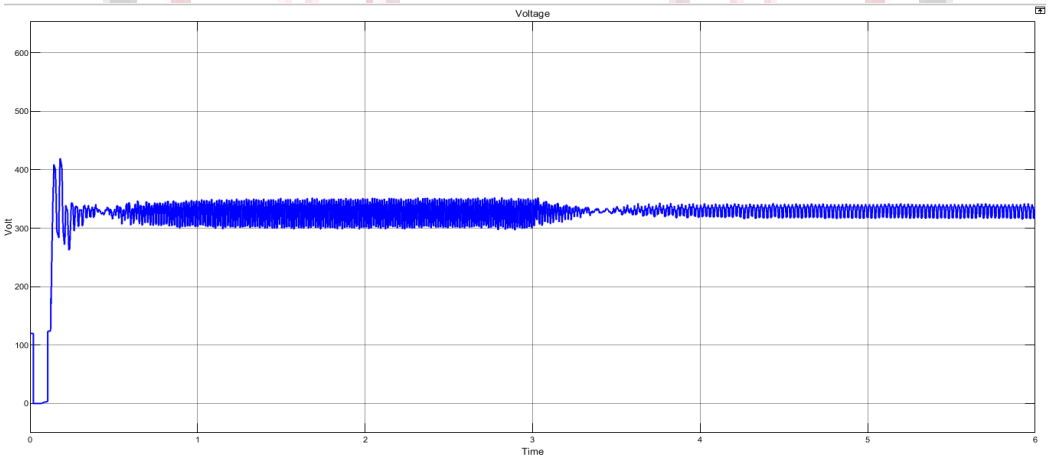

Figure 31 RMS voltage waveform representation in system 1 with basic V/F control (Deceleration mode)

To analyse the variations in the voltage waveform the RMS value is calculated which is represented in figure 31. The graphs shows variations in the waveform in the system having V/F speed control of motor during deceleration produced at the 3 sec.

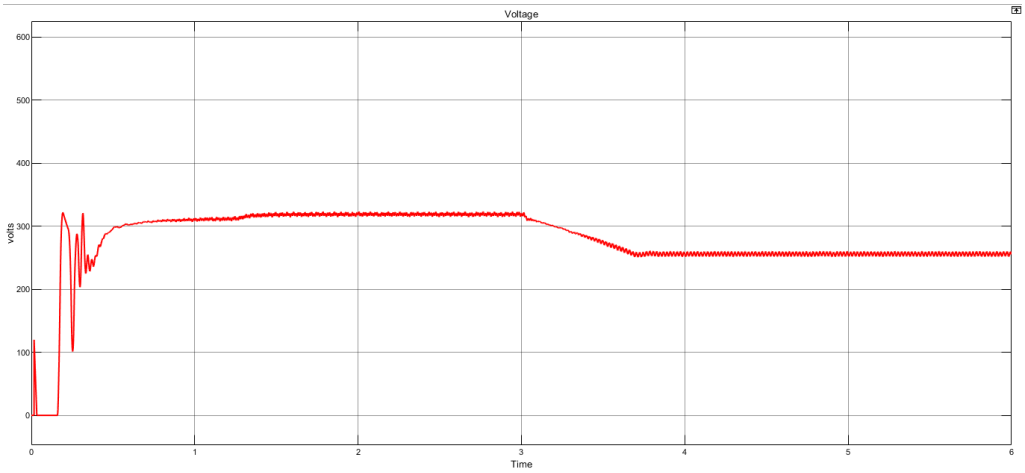

Figure 32 RMS voltage waveform representation in system 2 with parametric ant colony optimization control (Deceleration mode)

To analyse the variations in the voltage waveform the RMS value is calculated which is represented in figure 32. The graphs shows less variations in the waveform in the system having proposed parametric ant colony optimization control during deceleration at 3 sec and then after wards its stabilizes more as compared to waveform in V/F controller

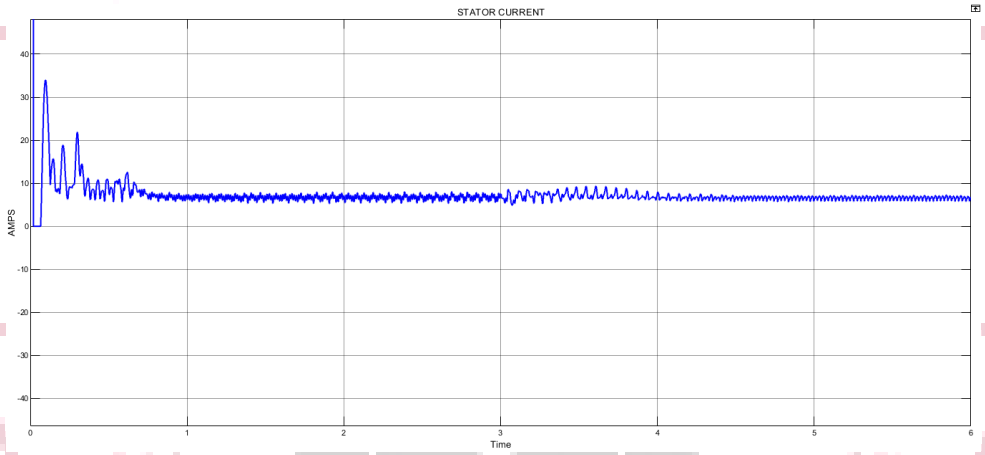

Figure 33 RMS current waveform representation in system 1 with basic V/F control (Deceleration mode)

To analyse the variations in the current waveform the RMS value is calculated which is represented in figure 33. The graphs shows variations in the waveform in the system having V/F speed control of motor during deceleration produced at the 3 sec.

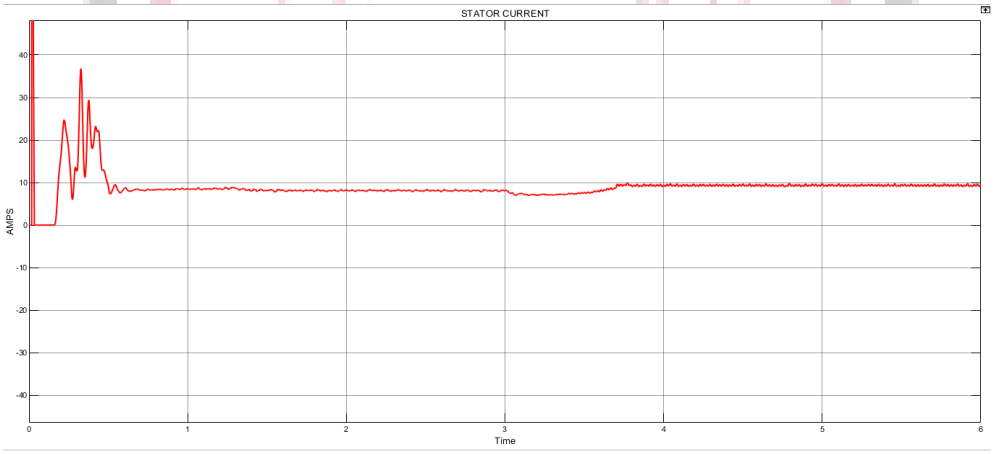

Figure 34 RMS current waveform representation in system 2 with parametric ant colony optimization control (Deceleration mode)

To analyse the variations in the current waveform the RMS value is calculated which is represented in figure 34. The graphs shows less variations in the waveform in the system having proposed parametric ant colony optimization control during deceleration at 3 sec and then after wards its stabilizes more as compared to waveform in V/F controller

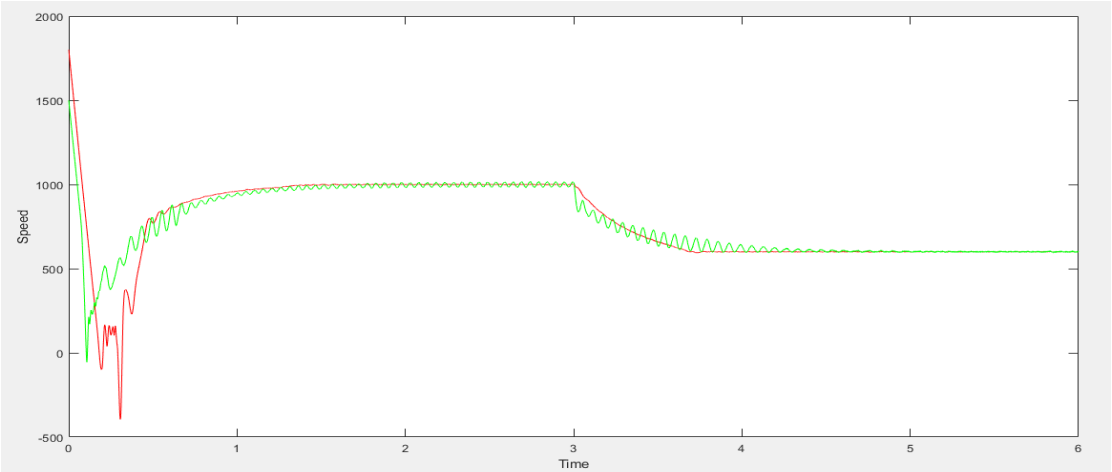

Figure 35 Comparative analysis of speeds in the two systems in case 3 (Deceleration mode)

The comparative analysis of the speeds in the two systems with different control has been depicted in the figure 35. The green graph represents the outcome from the system 1 with V/F control and the red graph is the speed of the motor in system 2 with proposed speed controller parametric ant colony optimization control during Deceleration produced at 3 sec.

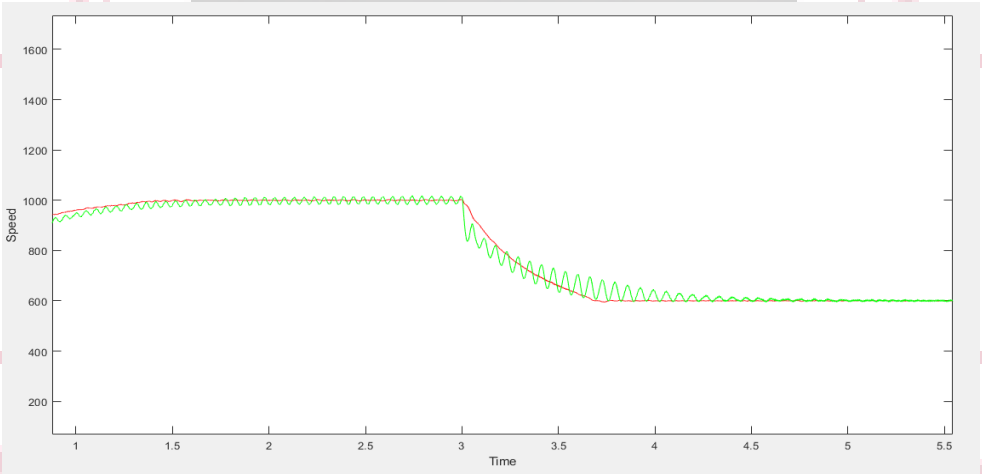

Figure 36 Close view of the speeds in two systems in case 3 (Deceleration mode)

Figure 36 is the comparative graph of speeds in the two systems with closer view of the variations produced in them during deceleration mode. The green graph as shown is having more variable waveform when the speed is reduced at 3 sec producing a spike and the red graph is decreasing more smoothly.

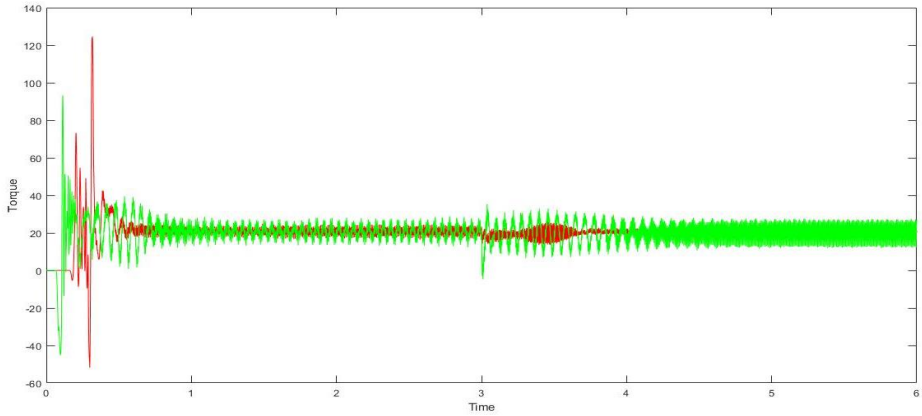

Figure 37 Comparative analysis of torques in the two systems in case 3 (Deceleration mode)

The comparative analysis of the torques in the two systems with different control has been depicted in the figure 37. The green graph represents the outcome from the system 1 with V/F control and the red graph is torque of motor in system 2 with proposed speed controller parametric ant colony optimization control during Deceleration produced at 3 sec.

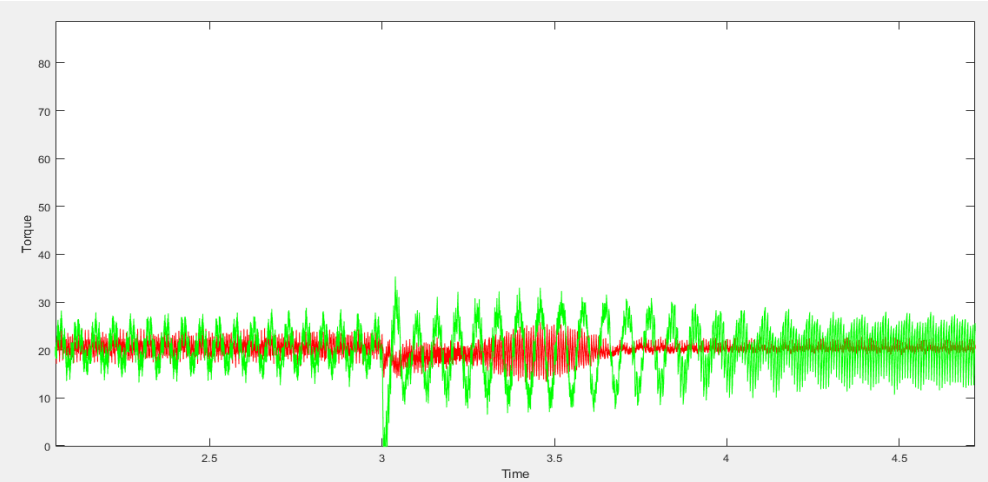

Figure 38 Close view of the torque in two systems in case 3 (Deceleration mode)

The comparative graph of torques in the two systems with closer view of the variations produced in them during deceleration mode is presented in figure 38. The green graph as shown is having more variable waveform when the speed is reduced at 3 sec producing a steep negative spike in torque also and the red graph of torque is more stable.

VI. CONCLUSION

This research provides valuable insights into the optimization and control of induction motors, addressing critical aspects of motor performance and efficiency. Through comprehensive modeling, simulation, and analysis, the study demonstrates the effectiveness of V/f control and ACO-based parameter optimization in enhancing motor stability and responsiveness across various operating conditions. The comparative assessments underscore the advantages of advanced control strategies in mitigating torque variations and improving overall system reliability. Moving forward, the findings of this study offer practical implications for industrial applications, paving the way for the development of more robust and adaptive induction motor control systems.

REFERENCES

[1] Abd-el-Malek, M.; Abdelsalam, A.K.; Hassan, O.E. Induction motor broken rotor bar fault location detection through envelope analysis of start-up current using Hilbert transform. Mech. Syst. Signal Process. 2017, 93, 332–350.

[2] Mehrjou, M.R.; Mariun, N.; Marhaban, M.H.; Misron, N. Rotor fault condition monitoring techniques for squirrel-cage induction machine—A review. Mech. Syst. Signal Process. 2011, 25, 2827–2848.

[3] Han, T.; Yang, B.-S.; Choi, W.-H.; Kim, J.-S. Fault diagnosis system of induction motors based on neural network and genetic algorithm using stator current signals. Int. J. Rotat. Mach. 2006, 2006, 61690.

[4] Toma, R. N., Prosvirin, A. E., & Kim, J. M. (2020). Bearing fault diagnosis of induction motors using a genetic algorithm and machine learning classifiers. *Sensors*, *20*(7), 1884.

[5] R. Marino, S. Peresada and P. Valigi, "Adaptive input-output linearizing control of induction motors," in *IEEE Transactions on Automatic Control*, vol. 38, no. 2, pp. 208-221, Feb. 1993, doi: 10.1109/9.250510.

[6] X. Liang, M. Z. Ali and H. Zhang, "Induction Motors Fault Diagnosis Using Finite Element Method: A Review," in *IEEE Transactions on Industry Applications*, vol. 56, no. 2, pp. 1205-1217, March-April 2020, doi: 10.1109/TIA.2019.2958908.

[7] Yakhni, M. F., Cauet, S., Sakout, A., Assoum, H., Etien, E., Rambault, L., & El-Gohary, M. (2023). Variable speed induction motors' fault detection based on transient motor current signatures analysis: A review. *Mechanical Systems and Signal Processing*, *184*, 109737.https://doi.org/10.1016/j.ymssp.2022.109737

[8] Aziz, A.G.M.A.; Abdelaziz, A.Y.; Ali, Z.M.; Diab, A.A.Z. A Comprehensive Examination of Vector-Controlled Induction Motor Drive Techniques. *Energies* 2023, *16*, 2854. https://doi.org/10.3390/en16062854

[9] Karupusamy, S., Mustafa, M.A., Jos, B.M. *et al.* Torque control-based induction motor speed control using Anticipating Power Impulse Technique. *Int J Adv Manuf Technol* (2023). https://doi.org/10.1007/s00170-023-10893-5

[10] S. P. Biswas, M. S. Anower, S. Haq, M. R. Islam, M. A. Rahman and K. M. Muttaqi, "A New Level Shifted Carrier Based PWM Technique for a Cascaded Multilevel Inverter Based Induction Motor Drive," in *IEEE Transactions on Industry Applications*, vol. 59, no. 5, pp. 5659-5671, Sept.-Oct. 2023, doi: 10.1109/TIA.2023.3279359.

[11] Karupusamy, S., Mustafa, M.A., Jos, B.M. *et al.* Torque control-based induction motor speed control using Anticipating Power Impulse Technique. *Int J Adv Manuf Technol* (2023). https://doi.org/10.1007/s00170-023-10893-5

[12] Tran, M. Q., Amer, M., Abdelaziz, A. Y., Dai, H. J., Liu, M. K., & Elsisi, M. (2023). Robust fault recognition and correction scheme for induction motors using an effective IoT with deep learning approach. *Measurement*, *207*, 112398. https://doi.org/10.1016/j.measurement.2022.112398

[13] Attar, H., Abu-Jassar, A.T., Lyashenko, V. *et al.* Proposed synchronous electric motor simulation with built-in permanent magnets for robotic systems. *SN Appl. Sci.* **5**, 160 (2023). https://doi.org/10.1007/s42452-023-05375-y

[14] Saxena, A., Kumar, R., Rawat, A. K., Majid, M., Singh, J., Devakirubakaran, S., & Singh, G. K. (2023). Abnormal Health Monitoring and Assessment of a Three-Phase Induction Motor Using a Supervised CNN-RNN-Based Machine Learning Algorithm. *Mathematical Problems in Engineering*, *2023*(1), 1264345.